Available online at www.sciencedirect.com
SCIENCE DIRECT®
Journal of Power Sources 130 (2004) 241–246
JOURNAL OF POWER SOURCES
www.elsevier.com/locate/jpowsour

Electrochemical characteristics and cycle performance of $LiMn_2O_4$/a-Si microbattery

Ki-Lyoung Lee [a], Ju-Young Jung [a], Seung-Won Lee [a], Hee-Soo Moon [a], Jong-Wan Park [a,b,*]

[a] *Division of Materials Science and Engineering, Hanyang University, 17 Haengdang-Dong, Seongdong-Gu, Seoul 133-791, South Korea*
[b] *Research Center for Energy Conversion and Storage, San 56-1, Shilim-dong, Kwanak-Gu, Seoul 151-742, South Korea*

Received 30 October 2003; accepted 24 November 2003

Abstract

A $LiMn_2O_4$ thin film and an amorphous Si (a-Si) thin film were prepared by radio-frequency (rf) magnetron sputtering. Each thin film was electrochemically evaluated by cyclic voltammetry (CV) and galvanostatic cycling. The rate of capacity fade on cycling was monitored as a function of the voltage window and current density. This was compared with the cycle performance of cathode and anode using two kinds of electrolyte, 1 M $LiPF_6$ in EC/DMC and PC, for 100 cycles. It was found that the discharge capacity of optimized $LiMn_2O_4$/a-Si full-cell reached 24 μAh/(cm^2-μm) in the first cycle, and a reversible capacity of about 16 μAh/(cm^2 μm) was still maintained after 100 cycles. In a voltage window of 3.0–4.2 V, $LiMn_2O_4$/a-Si full-cell exhibits relatively stable cycle performance compared to a voltage window of 2.75–4.2 V.

Keywords: Thin film; Amorphous silicon; $LiMn_2O_4$; rf Magnetron sputter; Full-cell

1. Introduction

Advances in micro-electro-mechanical systems (MEMS) technology have reduced the current and power requirements of some of these electronic devices to extremely low levels. This has made it possible to use thin-film solid-state microbatteries as power sources for these devices. Therefore, it is important to develop long-lasting and high-energy efficient microbatteries that would be suited for MEMS. Many types of the microbatteries and materials have been proposed [1–3].

$LiMn_2O_4$ is of great interest as a cathode material in Li secondary batteries due to its high voltage. $LiMn_2O_4$ thin films have been prepared by various deposition techniques such as chemical vapor deposition [4], radio-frequency (rf) sputtering [5], and PLD [6,7].

Most thin-film batteries generally have a Li metal anode [8–10]. In spite of its high constant voltage and high specific capacity (3860 mAh/g), Li metal is not suitable for use in micromechanic devices due to its low melting point (181 °C) and high reactivity with air during device processing [11,12]. Furthermore, it causes problems due to its reactivity with electrolytes, resulting in the formation of a dendritic Li phase after repeated charge–discharge cycling [13]. To solve these problems, attention has been shifted to Li metal alloys or metal oxides to deliver a higher anode capacity.

As an anode material, amorphous silicon (a-Si) offers a large increase of volumetric and gravimetric capacity due to its high lithium packing density and safe thermodynamic-potentials compared to carbonaceous materials like graphite [14–16]. In the case of $Li_{22}Si_5$, the theoretical capacity is 4200 mAh/g. The discharge capacity of a-Si during the electrochemical removal of Li is sufficiently flat, very similar to that of graphite, making it very attractive. However, the electrochemical performance of the electrode is much worse when the electrode thickness and particle size of active material increase. Therefore, a thin-film electrode could be suitable as a component for durable energy source.

In this work, we focused on a full-cell thin-film battery. Thus, we investigated electrochemical characteristics of each electrode ($LiMn_2O_4$, a-Si) and full-cell coupled with $LiMn_2O_4$/a-Si.

2. Experimental

$LiMn_2O_4$ films with a thickness of 2000 Å were prepared by rf magnetron sputtering with a mixture gas of Ar and O_2. Pt (2000 Å)/TiO_2 (200 Å)/SiO_2 (2000)/B-doped p-type

* Corresponding author. Tel.: +82-2-2290-0386; fax: +82-2-2298-2850.
E-mail address: jwpark@hanyang.ac.kr (J.-W. Park).

0378-7753/$ – see front matter © 2003 Elsevier B.V. All rights reserved.
doi:10.1016/j.jpowsour.2003.11.059

Si(1 0 0) wafers were used as substrates. To make the crystalline spinel-type $LiMn_2O_4$, the as-deposited films were annealed in a horizontal tube furnace in air at 750 °C for 120 min.

Si thin films were deposited by rf magnetron sputtering. The chamber was evacuated down to 5.3×10^{-4} Pa as a base pressure and a working pressure of 0.67 Pa was maintained with Ar gas. With a constant power density of 1.5 W/cm^2, Si thin films were deposited on Cu foils for a current collector (13 μm in foil thickness). The thickness of the Si thin film was controlled by deposition time. The deposition time was varied in order to obtain electrode thickness ranging from 220 to 680 Å. The crystallinity of the Si were characterized by X-ray diffractometry (RINT 2000, RIGAKU) with Cu Kα radiation at 40 kV and 100 mA, and a scan rate of 4°/min from 10 to 80° with 0.05° steps.

The thickness of the films was measured with a surface profilometer (Alpha-Step 500, TENCOR). The electrochemical measurements were conducted with a typical two-electrode cell. The half-cell for the cathode and the anode was composed of a Li metal foil as a counter electrode. Two kinds of electrolytes were examined: 1 M $LiPF_6$ solution in a propylene carbonate (PC) and 1 M $LiPF_6$ solution in a ethylene carbonate (EC)/dimethylecarbonate (DMC) (1:1, v/v) mixture. The cells were assembled in an Ar-filled glove box. Galvanostatic charge–discharge tests were performed with a cycle tester (WBCS 3000, WON A TECH). Each half-cell and full-cell was hence in various voltage windows. Cyclic voltammetry (CV) with various scan rates and number of cycles was also carried out.

3. Results and discussion

3.1. Characteristics of $LiMn_2O_4$ thin films

The charge–discharge curves for $LiMn_2O_4$ thin film measured between 3.8 and 4.2 V are given in Fig. 1. The first charge profile was found to differ considerably from other charge curves. This seems to correlate with the phase transition. The irreversible capacity loss at the first cycle is 24 μAh/(cm^2-μm) (45% loss). After the first cycle, the charge–discharge reactions are reversibly maintained for the subsequent cycles. CV shows typical two pairs of reversible oxidation and reduction peaks (Fig. 2). It is known that these two pairs of current peaks originate from two reversible phase–phase transitions of the $LiMn_2O_4$ during lithiation and delithiation processes.

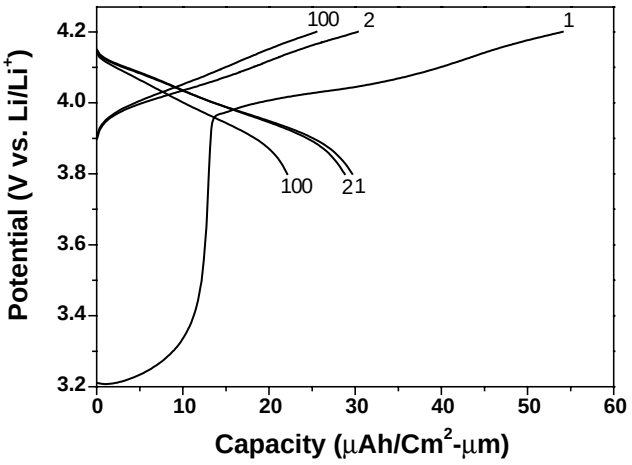

Fig. 1. Charge/discharge profiles of $LiMn_2O_4$ thin film.

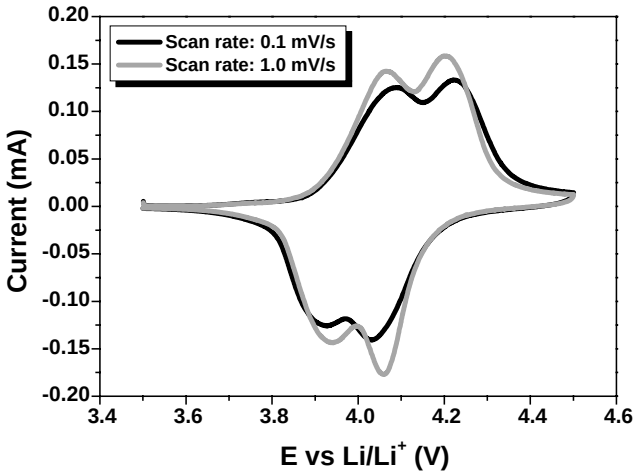

Fig. 2. The cyclic voltamogram of $LiMn_2O_4$ thin film.

3.2. Characteristics of a-Si thin film

No diffraction peaks, except those of the Cu foil (JCPDS 03-1005), could be detected by XRD (Fig. 3). Therefore, the deposited material was identified as an amorphous Si. Fig. 4 shows the charge–discharge curves of a-Si film measured between 0.01 and 1.0 V versus Li/Li$^+$ at a current density of 100 μA/cm^2. In the initial charge, the potential dropped rapidly to 0.26 V and maintained plateaus near 0.29 V, then gradually decreased to 0.01 V. This voltage-jumping

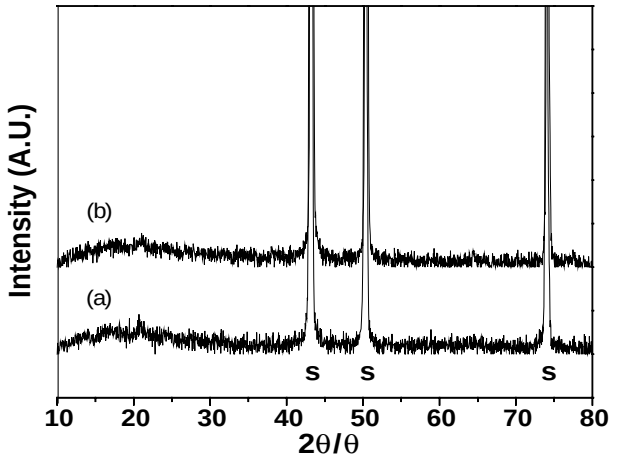

Fig. 3. XRD patterns of (a) a Cu foil and (b) a-Si thin film on a Cu foil ('S' denotes substrate).

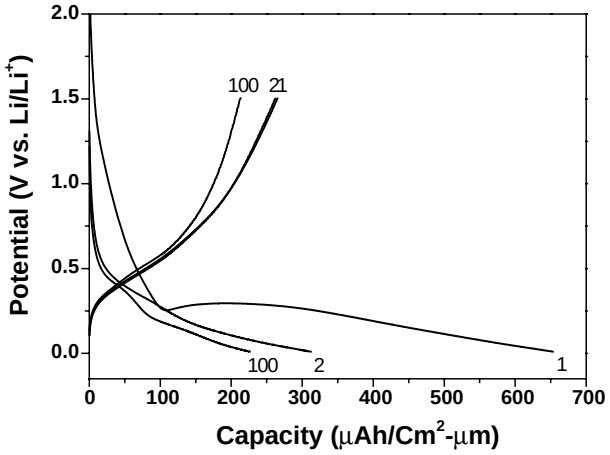

Fig. 4. Charge/discharge profiles of a-Si thin film.

behavior in the first cycle may be due to the inactive properties of Si film on the electrochemical reaction. The first irreversible capacity loss was about 60%. After the first cycle, the reversible charge–discharge reactions are maintained for the subsequent cycles.

The Li insertion/desertion into the film was done by CV (Fig. 5). From the results of Fig. 5a, it can be seen that Li insertion reaction occurred mostly at low potentials below 0.3 V. The broad peaks observed in the first cycle disappear at subsequent cycles. The irreversible reaction of the first cycle seems to be associated with formation of a solid electrolyte interface (SEI) layer or a dangling bond which is related to phase transformation [17]. Therefore, the significant reduction of the broad cathodic peak indicated that the irreversible reaction is suppressed by the maintenance of an equilibrium state in the second cycle. With an increasing number of cycles, the two cathodic peaks decrease gradually and the anodic peak at 0.48 V shifts toward a lower potential. The decrease of the cathodic peaks indicates that electrochemical reactivity was reduced upon cycling. The shift of the anodic peak may be due to gradual electrolyte penetration and more unimpeded Li transport into the inside of the electrode with repeated cycling. To examine the kinetics of the electrochemical processes, the CV of a-Si thin film was observed at scan rate from 0.1 to 2.0 mV/s (Fig. 5b). As the scan rate increased, cathodic/anodic current significantly increased and the anodic peak shifts to higher potential. Result of Song et al. [18] was not consistent with our study. Song et al. [18] suggested that an increase in the scan rate is correlated with a reduction of peak height in the CV because only the film surface participates in the reaction. However, the a-Si electrode used in our study has a smaller thickness to that (1370 Å) used in Song's study. Therefore, the boundary between the surface and bulk does not exist. Hence, with increasing scan rate, peak height increased. On the other hand, the potential shift with scan rate in this study also indicates increased kinetic polarization and internal resistance.

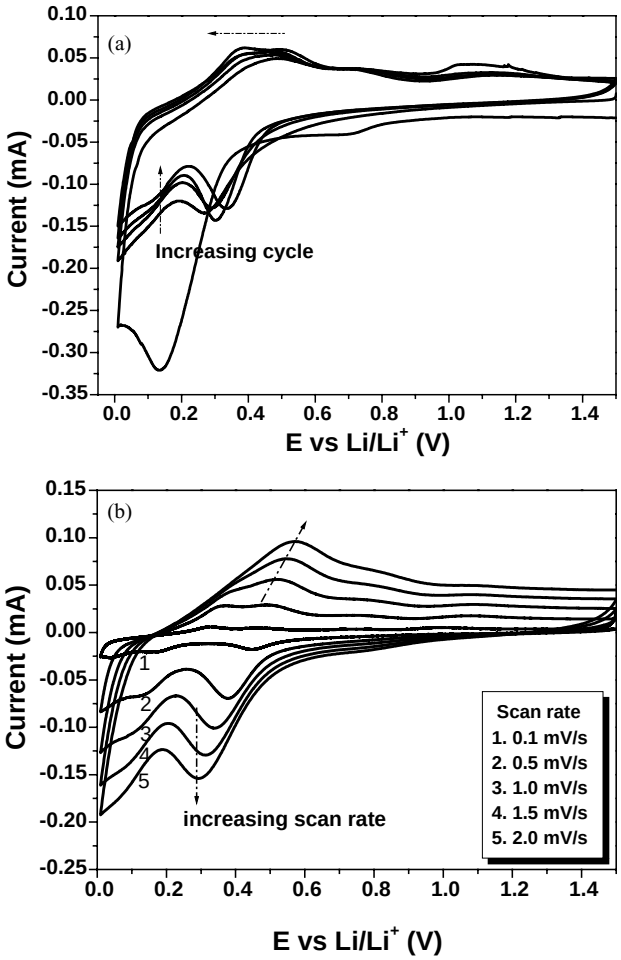

Fig. 5. The cyclic voltamogram of Si thin film with (a) cycle number and (b) scan rate.

Fig. 6 shows the relationship between the discharge capacity and the cycle number when cells were cycled between three different voltage limits, 0.0–1.5, 0.01–1.5, and 1.0–1.5 V; and current density, 100, 50, and 10 μA/cm^2. When the current density was 100 μA/cm^2, the initial discharge capacities were about 280, 187, and 138 μAh/(cm^2-μm), respectively. The discharge capacity maintained more than 90% of initial capacity during 30 cycles. Decreasing the current density from 100 to 50 μA/cm^2, increased the discharge capacity in all voltage windows. In particular, in the range of 0.0–1.5 V, the reversible capacity of the a-Si electrode increased significantly to nearly 330 μAh/(cm^2-μm). When a current density of 10 μA/cm^2 was applied, the discharge capacity increased considerably. However, when cycled over the full compositional range, the capacity fade is relatively fast. This capacity fade is attributed to volumetric changes that are more severe when the electrodes are fully lithiated. Even though the current density returned to its initial state, the capacity did not recover, except in the 0.01–1.5 V range. Therefore, we found that the stable voltage window of a-Si anode was 0.01–1.5 V.

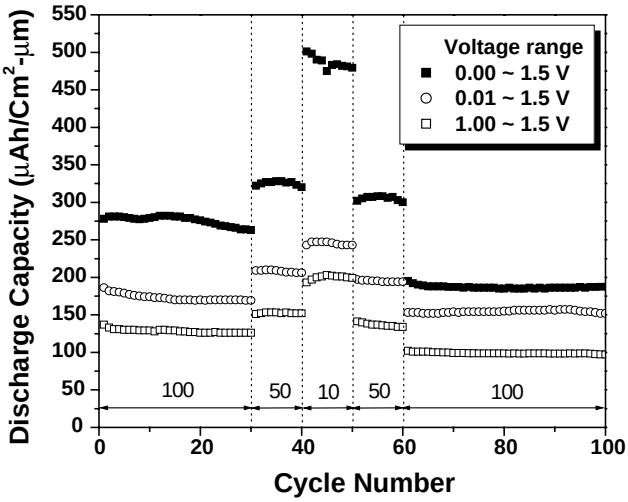

Fig. 6. The discharge capacity according to a variety of current density and voltage range.

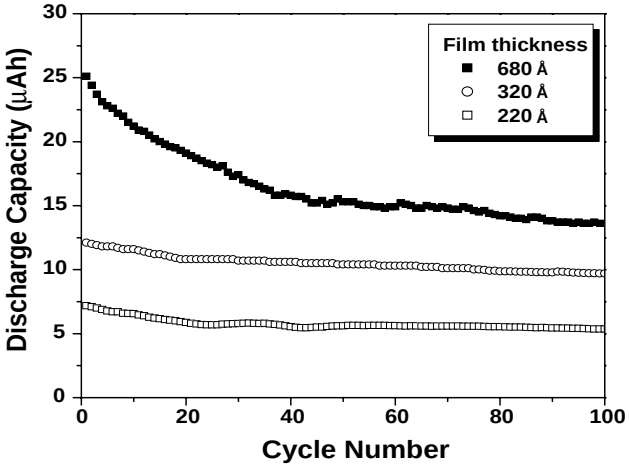

Fig. 8. The discharge capacity according to thickness of a-Si thin film.

Fig. 7 compares the cycle performance of cathode and anode using two kinds of electrolyte, 1 M $LiPF_6$ in EC/DMC and PC, for 100 cycles. As shown in Fig. 7a, there is no significant difference between the two solvent systems used except for initial capacity. However, in the anode system (Fig. 7b), capacity declines upon cycling, especially in the EC/DMC solvent. PC solvent was found to be more appropriate than EC/DMC solvent when using a-Si anode.

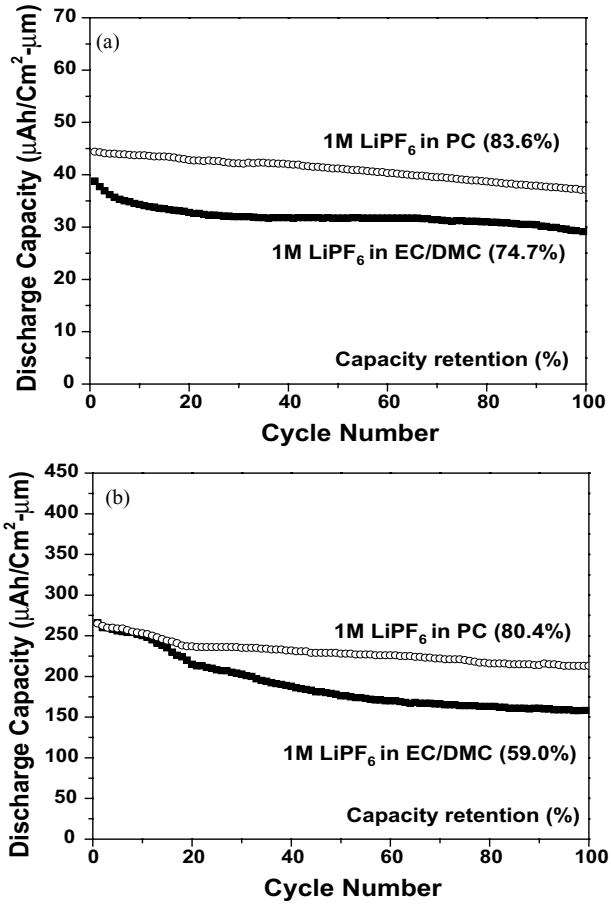

Fig. 7. Cycle performance according to electrolyte (1 M $LiPF_6$ in EC/DMC and PC): (a) $LiMn_2O_4$ thin film and (b) a-Si thin film.

Fig. 8 shows the effect of film thickness on the cyclic performance at a constant current density of 100 μA/cm^2. Initial discharge capacities of the films are relatively proportionate to film thickness, namely the amount of deposited Si. Films with thickness of 220 and 320 Å remain stable for 100 cycles. The capacity of a-Si films was maintained at approximately 5 and 10 μAh during 100 cycles. However, the capacity of the 680 Å film abruptly drops from 25 to 14 μAh. It is generally known that the electrochemical performance is much worse when the two-dimensional film is thick. The reasons why such problems occur may be the increased diffusion length of Li or the increase of resistance and stress damage in the film.

3.3. Electrochemical characteristics of the full-cell

To prevent the capacity loss of the $LiMn_2O_4$ thin film by irreversible behavior of a-Si thin film in the initial cycle, electrochemical lithiation of a-Si thin film was carried out. Before it was applied to the full-cell, a-Si anode was cycled for five cycles. Then, the components of the cell (especially anode part) were carefully disassembled in an Ar-filled glove box, and then $LiMn_2O_4$/1 M $LiPF_6$ in PC/a-Si full-cells were assembled. Fig. 9 shows the cycle performance of the full-cells made from cycled a-Si anode and fresh a-Si anode. The full-cell composed of the cycled a-Si anode exhibits better capacity and cyclability compared to the fresh a-Si anode. Therefore, the subsequent full-cell experiments used the lithiated a-Si anode. In this study, many full-cells with various anode thickness (220, 320, and 680 Å) and electrolyte were tested. However, we have not yet found any tendency with configuration condition for the full-cell. In

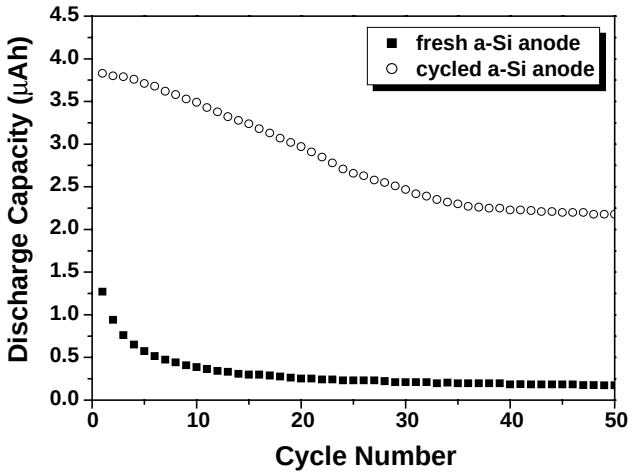

Fig. 9. Cycle performance of full-cells made from (a) cycled a-Si anode and (b) fresh a-Si anode.

this study, film thickness of anode had no distinct effect on capacity and cycle performance. More research is needed in this area in order to improve the performance of thin-film full-cells.

Fig. 10 shows the charge/discharge capacity of optimized full-cell as a function of cycle number. It was found that the discharge capacity of the cell in the first cycle reached 24 μAh/(cm^2-μm), and a reversible capacity of about 16 μAh/(cm^2-μm) can be achieved. Coulombic efficiency was found to be about 42% in the first cycle and 93% after 20 cycles, respectively.

The charge/discharge voltage profiles of the half-cell (for cathode) and the full-cell made from the a-Si anode at second cycles are shown in Fig. 11. There is a voltage drop by voltage difference between the Li metal and the a-Si anode. The cycle properties were monitored as a function of the voltage window (Fig. 12). The capacity fading highly takes place when cells are cycled between 2.75 and 4.2 V.

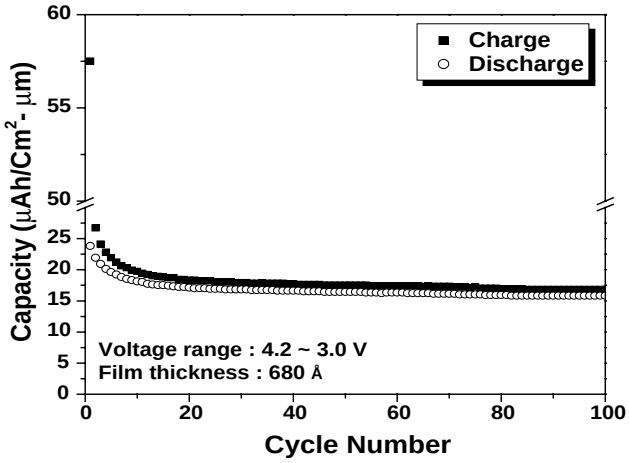

Fig. 10. Cycle performance of $LiMn_2O_4$/1 M $LiPF_6$ in PC/a-Si.

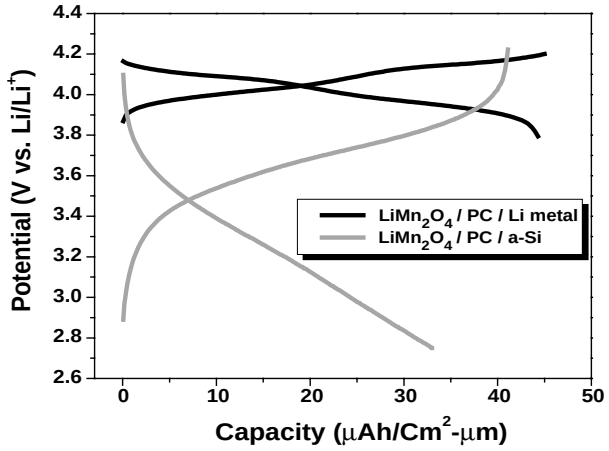

Fig. 11. The charge/discharge voltage profiles of the half-cell (for cathode) and full-cell at second cycles.

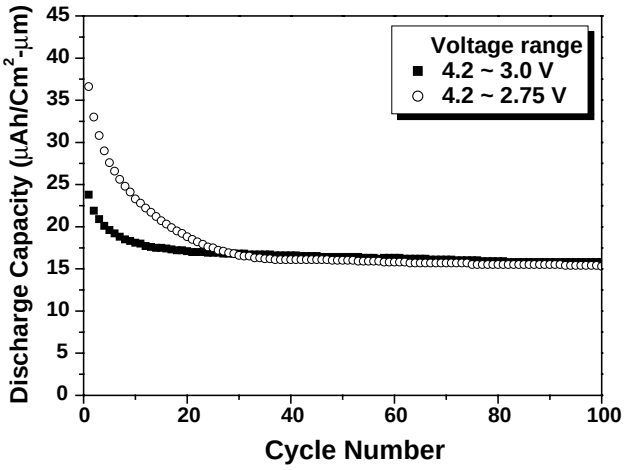

Fig. 12. The discharge capacity of full-cell according to voltage range.

4. Conclusions

A $LiMn_2O_4$ thin film and an amorphous Si thin film were prepared by rf magnetron sputtering. Electrochemical characteristics of each component and a full-cell were examined. The stable voltage window on the a-Si anode was found to be 0.01–1.5 V. A long cycle life of the cell was exhibited even in a PC electrolyte. The full-cell composed of the cycled a-Si anode exhibits better capacity and cyclability compared to a fresh a-Si anode. It was found that the discharge capacity of the cell in the first cycle reached 24 μAh/(cm^2-μm), and the reversible capacity of about 16 μAh/(cm^2-μm) was still maintained after 100 cycles.

Acknowledgements

This work was supported by KOSEF through the Research Center for Energy Conversion and Storage.

References

[1] B. Wang, J.B. Bates, F.X. Hart, B.C. Sales, R.A. Zuhr, J.D. Robertson, J. Electrochem. Soc. 143 (1996) 3203.
[2] B.J. Neudecker, R.A. Zuhr, J.B. Bates, J. Power Sources 81–82 (1999) 27.
[3] B.J. Neudecker, N.J. Dudney, J.B. Bates, J. Electrochem. Soc. 147 (2000) 517.
[4] P. Liu, J.-G. Zhang, J.A. Turner, C.E. Tracy, D.K. Benson, J. Electrochem. Soc. 146 (1999) 2001.
[5] T. Brousse, P. Fragnaud, R. Marchand, D.M. Schleich, O. Bohnke, A.K. West, J. Power Sources 68 (1997) 412.
[6] M. Morcrette, P. Barboux, J. Perriere, T. Brousse, Solid State Ionics 112 (1998) 249.
[7] D.S. Ginley, J.D. Perkins, J.M. McGraw, P.A. Parilla, Mat. Res. Soc. Symp. Proc. 496 (1998) 293.
[8] J.B. Bates, N.J. Dudney, G.R. Gruzalski, R.A. Zuhr, A. Choudhury, C.F. Luck, J.D. Robertson, J. Power Sources 43 (1993) 103.
[9] S.D. Jones, J.R. Akrigde, F.K. Shokoohi, Solid State Ionics 69 (1994) 357.
[10] J.B. Bates, G.R. Gruzalski, N.J. Dudney, C.F. Luck, Xiaohua Yu, Solid State Ionics 70–71 (1994) 619.
[11] P. Birke, S. Doring, W. Weppner, in: Proceedings of the 11th International Conference on Solid State Ionics, vol. 70, 1997.
[12] B.J. Neudecker, N.J. Dudney, J.B. Bates, J. Electrochem. Soc. 147 (2000) 517.
[13] R.A. Huggins, J. Power Sources 81–82 (1999) 13.
[14] J.O. Besenhard, J. Yang, M. Winter, J. Power Sources 68 (1997) 87.
[15] V. manev, I. Naidenov, B. Puresheva, G. Pistoia, J. Power Sources 57 (1995) 133.
[16] S. kuwabata, N. Tsumura, S. Goda, C.R. Martin, H. Yoneyama, J. Electrochem. Soc. 145 (1998) 1415.
[17] Hong Li, Xuejie Huang, Liquan Chen, Zhengang Wu, Yong Liang, Electrochem. Solid-State Lett. 2 (1999) 547.
[18] Seung-Wan Song, Kathryn A. Striebel, Ronald P. Reade, Gregory A. Roberts, J. Cairns, J. Electrochem. Soc. 150 (2003) A121.